





## Article

# Experimental Study for the Evaluation of Titanium Disc Decontamination and Osseointegration in the Rabbit Tibia Model

Hye Jin Kim <sup>1</sup> , Kyoungseok Choi <sup>1</sup>, Chulyoung Park <sup>1</sup>, Ji Hyun Kim <sup>1</sup> , Jaeyoung Ryu <sup>1</sup> , Seunggon Jung <sup>1</sup>, Min-Suk Kook <sup>1</sup> , Hee-Kyun Oh <sup>1</sup>, Yun Kyong Lim <sup>2</sup>, Joong-Ki Kook <sup>2</sup> and Hong-Ju Park <sup>1,\*</sup>

- <sup>1</sup> Department of Oral and Maxillofacial Surgery, School of Dentistry, Dental Science Research Institute, Chonnam National University, Gwangju 61186, Republic of Korea; dateddy0519@gmail.com (H.J.K.); jsandsk2@naver.com (K.C.); dentrader20@gmail.com (C.P.); cathy1555@gmail.com (J.H.K.); ryu@jnu.ac.kr (J.R.); seunggon.jung@jnu.ac.kr (S.J.); omskook@jnu.ac.kr (M.-S.K.); hkoh@jnu.ac.kr (H.-K.O.)
- <sup>2</sup> Korean Collection for Oral Microbiology and Department of Oral Biochemistry, School of Dentistry, Chosun University, Gwangju 61452, Republic of Korea; dbsruddl77@hanmail.net (Y.K.L.); jkkook@chosun.ac.kr (J.-K.K.)
- \* Correspondence: omspark@jnu.ac.kr

**Abstract:** Peri-implantitis is an inflammatory lesion leading to bone destruction resulting from bacterial infection and biofilm formation. Treatments of peri-implantitis aim at bacterial controls and decontamination to promote re-osseointegration. The present study aimed to assess the decontamination of biofilm and the osseointegration of titanium discs in a rabbit tibia model. Discs were immersed in culture medium inoculated with *Staphylococcus aureus* and incubated at 37 °C for 24 h and allocated to different treatments (n = five per group). The decontamination methods were an air-polishing system, 0.12% chlorhexidine rinse, and Er:Yag laser treatments. Each disc from the experimental groups was observed using scanning electron micrography. The rest of the discs were then implanted in four male New Zealand rabbits. Histological and radiographic evaluations were performed. For the quantification of bone density in radiographic data, the fractal dimension (FD) and mean grayscale value (GV) were measured. The Kruskal–Wallis test was used to compare bone density ( $p < 0.05$ ). Statistically significant differences in FD were observed between the air-polishing treatment with chlorhexidine rinse and the air-polishing treatment with chlorhexidine rinse and Er:Yag laser treatment compared to the contaminated group ( $p < 0.05$ ). Also, there were statistically significant differences in the results obtained for the group undergoing air-polishing treatment with chlorhexidine rinse and Er:Yag laser treatment compared to the contaminated group ( $p < 0.05$ ). The decontamination method using air polishing treatment, chlorhexidine rinse, and Er:Yag treatment showed favorable osseointegration with good bone quality.

**Keywords:** air polishing treatment; Er:Yag laser treatment; osseointegration



**Citation:** Kim, H.J.; Choi, K.; Park, C.; Kim, J.H.; Ryu, J.; Jung, S.; Kook, M.-S.; Oh, H.-K.; Lim, Y.K.; Kook, J.-K.; et al. Experimental Study for the Evaluation of Titanium Disc Decontamination and Osseointegration in the Rabbit Tibia Model. *Appl. Sci.* **2023**, *13*, 11177. <https://doi.org/10.3390/app132011177>

Academic Editors: Takehito Ouchi and Shogo Maekawa

Received: 12 September 2023

Revised: 2 October 2023

Accepted: 8 October 2023

Published: 11 October 2023



**Copyright:** © 2023 by the authors. Licensee MDPI, Basel, Switzerland. This article is an open access article distributed under the terms and conditions of the Creative Commons Attribution (CC BY) license (<https://creativecommons.org/licenses/by/4.0/>).

## 1. Introduction

Osseointegrated dental implants are an effective treatment for missing teeth with high survival rates. However, peri-implantitis is one of the major complications for supporting bone destruction leading to a loss of the implant [1–4]. Peri-implantitis is an inflammatory lesion affecting the surrounding tissue of an osseointegrated implant resulting from bacterial infection and biofilm formation [5–7]. Treatments of peri-implantitis aim at bacterial controls and decontamination to promote re-osseointegration [3,7,8]. Effective decontamination of the infected surface is crucial, and various decontamination methods have been proposed in the literature [1,4,9–11]. Despite numerous suggested effective decontamination methods from multiple studies, a consensus on gold standards for peri-implantitis treatments remains elusive. Additionally, challenges persist in the re-osseointegration of previously contaminated implants [1,2].

Decontamination methods for peri-implantitis include mechanical debridement using scalers and ultrasonic scalers with plastic, metal, or carbon fiber tips, air-polishing systems, and lasers. Alternative approaches to treatment comprise disinfection modalities, such as antiseptics, photothermal laser disinfection, photodynamic therapy, the administration of local or systemic antibiotics, or a combination of these methods [5,12–15].

Air-polishing therapy is one of the mechanical decontamination methods, involving the use of low-abrasive powders, water, and pressurized air to remove biofilm from implant surfaces through abrasion. Various types of abrasive powders are available, including sodium bicarbonate, glycine salt, aluminum trioxide, and calcium carbonate [16]. Compared to sodium bicarbonate powders, *in vitro* and *in vivo* studies have demonstrated that glycine powders are less abrasive, safe, and effective for biofilm removal [17–19].

Various types of lasers, including neodymium-doped yttrium aluminum garnet (Nd:YAG), erbium-doped yttrium aluminum garnet (Er:YAG), erbium–chromium-doped yttrium scandium gallium garnet (Er,Cr:YSGG), and carbon dioxide (CO<sub>2</sub>) lasers, have been used for periodontal treatments [7,20]. The erbium family lasers that produce middle infrared lasers, Er:YAG and Er,Cr:YSGG, have gained attention for their efficacy in treating peri-implantitis [21]. The Er:YAG laser has demonstrated potent bactericidal properties and an ability to neutralize bacterial toxins against periodontal pathogens [7,15,22].

Chlorhexidine gluconate is a diphenyl compound with broad-spectrum antibacterial properties, acting by altering bacterial cell membranes and causing leakage and subsequent cell destruction [23]. Chlorhexidine is reported as a chemical antiseptic that can be used as a decontamination method in peri-implantitis [16]. Chlorhexidine demonstrates a bactericidal effect and the inhibition of biofilm formation [20]. Also, chlorhexidine has been shown to contribute to re-osseointegration in peri-implantitis lesions [16,24].

Bone density quantifies the size of the marrow space relative to the bone volume and serves as a valuable metric for assessing the quality of osseointegration in decontaminated implants [25]. The fractal dimension (FD) is a quantitative value for evaluating the trabecular bone pattern [26]. This method involves statistical analysis of the structural patterns in the fractal dimension and is independent of projection geometry and radiodensity; thus, it is widely employed in the dental field, including the evaluation of implant stability [27,28]. As inflammation in the bone progresses, the trabecular bone is destroyed, and lower FD values are obtained [25]. Also, the mean grayscale value (GV) serves as the metric for quantifying bone density measurements [25,29]. The mean GV demonstrates the intensity of attenuated X-rays using a numerical scale. In computed tomography (CT) using three-dimensional reconstruction, the obtained grayscale is utilized for the quantification and evaluation of regenerated osseous tissue [30].

This study aimed to assess the efficacy of decontamination methods using an air-polishing system, chlorhexidine rinse, and an Er:Yag laser on biofilm-covered titanium discs, utilizing a scanning electron microscope. Additionally, it aimed to evaluate the osseointegration based on bone density measurements after implantation on the tibia of rabbits, employing the radiographic and histologic data.

## 2. Materials and Methods

### 2.1. Specimens

Titanium alloy (Ti-6Al-4V) discs, with a diameter of 8 mm and a thickness of 3 mm, which had been sandblasted with Al<sub>2</sub>O<sub>3</sub> and etched with hydrogen chloride and sulfuric acid, were used. The *Staphylococcus aureus* (*S. aureus*) KCOM 1025 (Korean Collection for Oral Microbiology, Gwangju, Republic of Korea) was cultured in brain heart infusion broth (BHI, Becton, Dickinson and Company, Sparks, MD, USA). For the purpose of contamination, each sterile disc was immersed in BHI broth medium inoculated with *S. aureus* and incubated at 37 °C for 24 h.

## 2.2. Decontamination Method

An Er:YAG laser with a wavelength of 2940 nm (Anybeam™ Top EN Plus, POINT ANYBEAM Co., Ltd., Seoul, Republic of Korea) was used to irradiate on the surfaces of the discs. The laser was set for curettage or implant disinfection based on the manufacturer's instructions. An air-polishing system with glycine powder (Perio-Mate, NSK-Nakanishi Inc., Kanuma Tochigi, Japan) was applied for 5 s with a 10 mm distance from the specimens, according to the manufacturer's instructions. The discs were rinsed with 0.12% chlorhexidine (Osstem Pharma. Co., Ltd., Seoul, Republic of Korea) for 1 min (Figure 1).

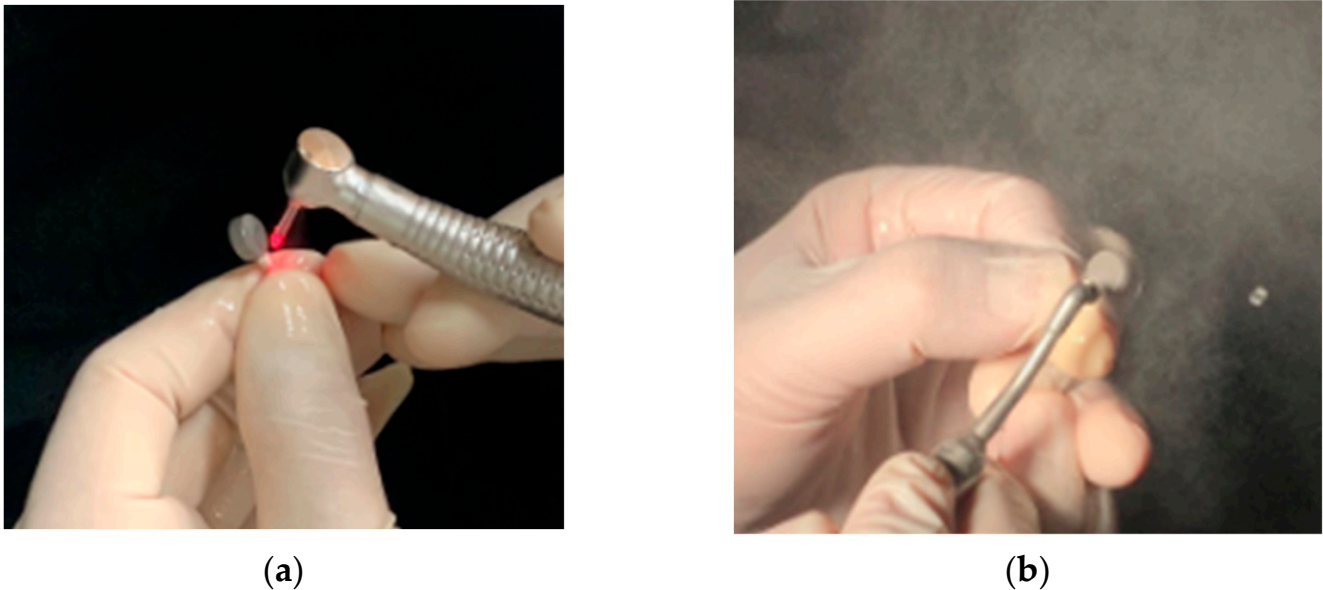


**Figure 1.** Decontamination using an (a) Er:Yag laser and (b) air-polishing system.

## 2.3. Experimental Groups

Sterile titanium discs were allocated into two groups: those incubated with *S. aureus* coated with biofilm or without biofilm. The titanium discs without biofilm and decontamination treatment remained sterile and were allocated to the negative control group, group N. Biofilm-coated titanium discs were divided according to the treatments used: an air-polishing system (A), an Er:YAG laser (E), and 0.12% chlorhexidine rinse (C) (Table 1). Titanium discs with biofilm but without any decontamination treatments were allocated to the positive control group, group P.

**Table 1.** Experimental groups.

Group	Biofilm	Treatment	Number of Discs
N	No	No	5
P	Yes	No	5
A	Yes	Air-polishing system	5
AC	Yes	Air-polishing system with 0.12% chlorhexidine rinse	5
ACE	Yes	Air-polishing system with 0.12% chlorhexidine rinse and an Er:Yag laser	5

N = Negative control group; P = Positive control group; A = Air-polishing treatment group; AC = Air-polishing treatment with chlorhexidine rinse group; ACE = Air-polishing treatment, chlorhexidine rinse, and Er:Yag laser treatment group.

## 2.4. Surface Tomography

Each disc from the experimental groups was evaluated using a scanning electron microscope (Hitachi SU8230, with a cold-field-emission cathode of 5 kV and a distance

of 15 mm, Hitachi, Tokyo, Japan) (SEM, Hitachi, Japan) to assess the presence of *S. aureus* on the surface after each treatment. All specimens were platinum-coated, with a layer thickness of approximately 50 nm, and observed under a magnification of 5000 $\times$ .

### 2.5. Animal Experiments

Four male New Zealand white rabbits, weighing 3.0–3.5 kg, were used. The rabbits were obtained from Da-mool Science (Daejeon, Republic of Korea) and reared at the Laboratory Animal Research Center of Chonnam National University. The animal care and experimental procedures were approved by the Institutional Animal Care and Use Committee of Chonnam National University Hospital (CNUHIACUC-22017).

Anesthesia was induced using ketamine and xylazine (60 mg/kg and 10 mg/kg intramuscularly, respectively), and the hind legs were shaved. Infiltration anesthesia (lidocaine 2% and epinephrine 1:100,000) was used at the experimental sites. Surgeries were performed by an experienced surgeon. The surgical sites were accessed with 3 cm long incisions through the skin and fascia. Bone surfaces were exposed using an elevator. The discs were placed following site preparation using saline-cooled 3.0 mm round burs. Three discs were placed into each tibial metaphysis (Figure 2). The experimental and control discs were alternated between the left and right hind limbs. The fascia and skin were closed in layers with interrupted sutures, as appropriate, using resorbable (Vicryl 4.0, Ethicon, Inc., Raritan, NJ, USA) and nonresorbable (Nylon 4/0, AILEE CO., Seoul, Republic of Korea) materials.

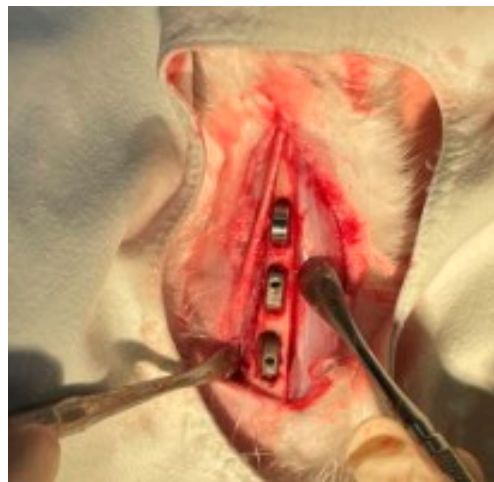


**Figure 2.** Disc implantation on the tibia of rabbits.

No postoperative complications, such as pus discharge or swelling, were found in the rabbits. The rabbits were sedated and euthanized 6 weeks after surgery with a lethal dose of a potassium chloride injection. The experimental sites of the tibia were collected and fixed in 10% buffered formalin.

### 2.6. Histologic Findings

The specimens were infiltrated with a chemical curing resin (methacrylate-based) and embedded with benzoyl peroxide. The blocks were cut along the longitudinal axis of the discs and sectioned at a 4  $\mu$ m thickness along the sagittal plane through the center of the implant. The sections underwent hematoxylin and eosin staining (H&E). The bone formation around the discs was observed using light microscopy (Olympus, Tokyo, Japan) under 12.5 magnifications.

### 2.7. Experimental Group Micro-Computed Tomography (Micro-CT) Processing and Analysis

Micro-CT data were acquired using a tube voltage of 110 kVp and a current of 50 A (SMX-225CT, InspecIo, Seoul, Republic of Korea), and the data were reconstructed using

Mimics (Materialise, Leuven, Belgium). For FD calculation, the images corresponding to the histologic sections were collected and analyzed using the ImageJ program (Wayne Rasband, National Institutes of Health, Bethesda, MD, USA). Rectangular regions of interest (ROIs,  $25 \times 100$  pixels) were selected between the disc and the cortical bone beneath the superior cortical border. FDs were calculated using the algorithm developed by White and Rudolph [26,27]. A Gaussian filter (sigma = 35 pixel) was applied to each image to leave large-scale details, and the blurred image was subtracted from the original image. Then, 128 pixels were added, and the image was converted to a binary image to obtain the trabecular pattern. The image was eroded, dilated, and skeletonized, and then the FD was calculated using the box-counting method (Figure 3). On the other hand, the Mimics program was used for measurements of the mean GV. The segmentation of the disc and the tibia was accomplished. Using the morphology operation tool, the ROI was set for the surrounding 20 pixels of the disc restricted by the tibia and calculated. The mean GV of the ROI was measured as the quantification of bone density (Figure 4).

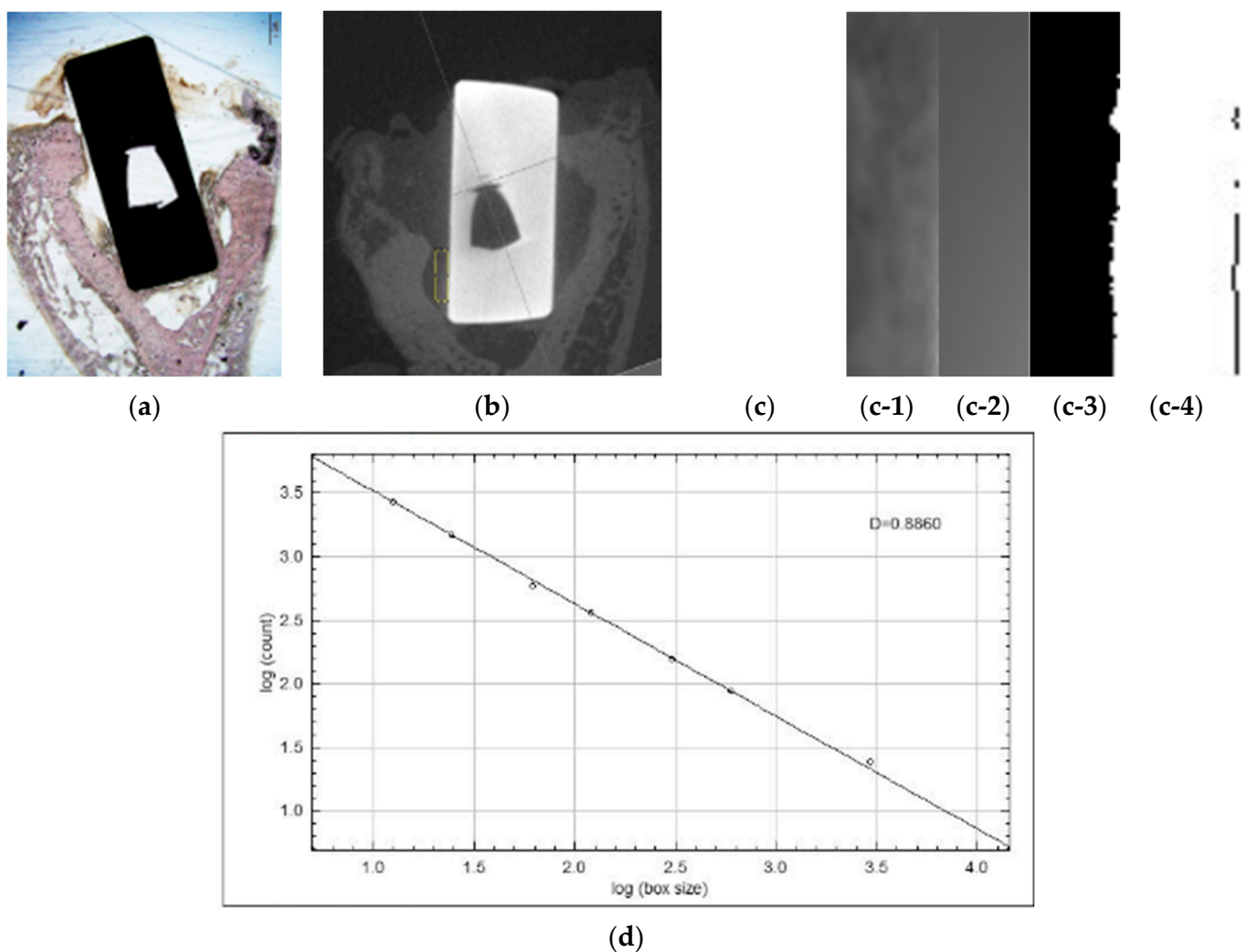


**Figure 3.** Images of the (a) histopathologic specimen; (b) ROI (yellow rectangle) used to calculate the FD in the micro-CT image corresponding to the histopathologic image; (c) process of FD calculation; (c-1) ROI image; (c-2) image with a Gaussian filter; (c-3) binary image; (c-4) skeletonized image; and (d) FD analysis using the box-counting method.

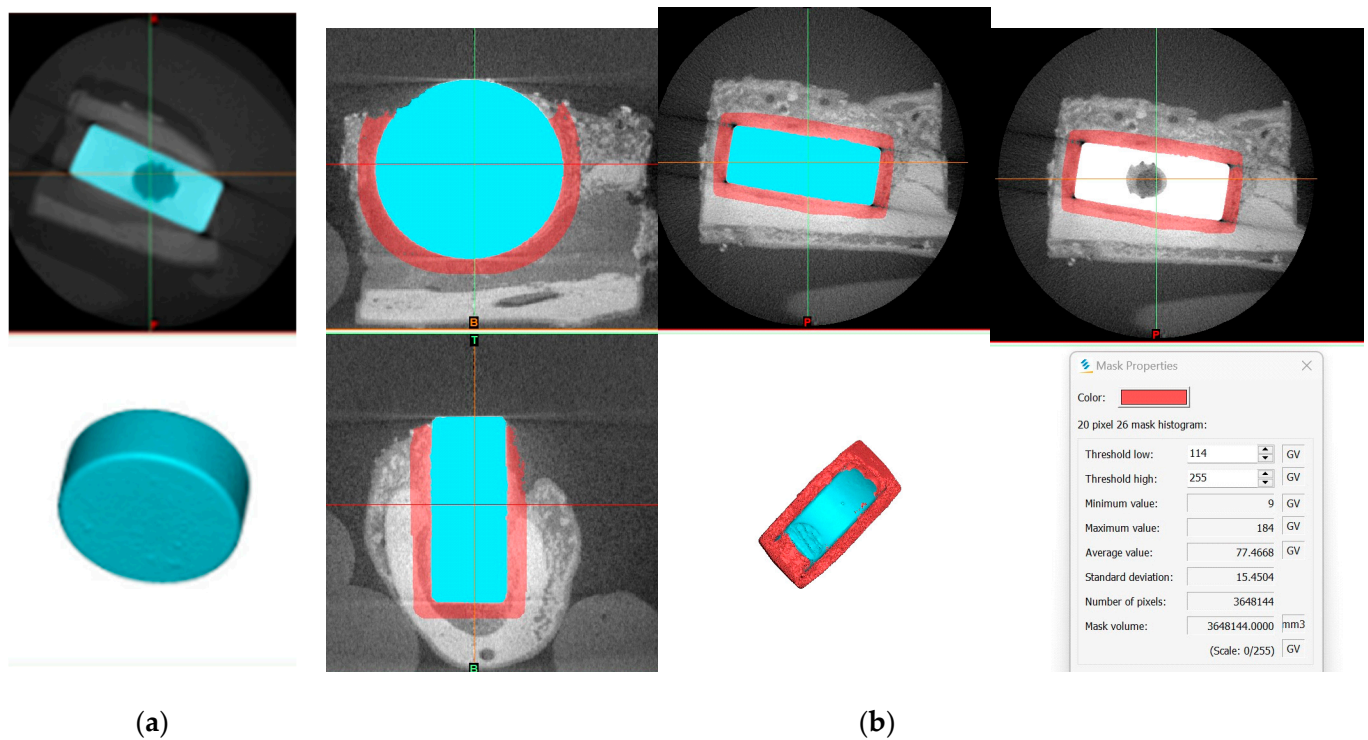


**Figure 4.** Images of the (a) segmented disc in blue and (b) segmentation of ROI in red using a morphology operation tool and mean GV measurements in properties.

### 2.8. Statistical Analysis

Based on a priori sample size calculation conducted using a statistical software (G\*Power 3.1.9.7, Dusseldorf, Germany), a minimum sample size of 20 was determined, with a significance level of 0.05, a power of 0.8, and a large effect size. Within each treatment group, the measured FD and GV were assessed to determine the normality of the data using the Shapiro–Wilkson test, and the values of the groups were compared using the Kruskal–Wallis test with the Conover test for multiple-comparison. The Holm method was used for the adjustment of the  $p$ -value. Statistical analysis was conducted using the “R” statistical package version 4.2.3 (R Foundation for Statistical Computing, Vienna, Austria). The significance level was set to  $p < 0.05$ .

## 3. Results

### 3.1. Surface Tomography

The SEM images for each experimental group of specimens were captured at a magnification of 5000 $\times$  (Figure 5). The negative control group disc showed a clear surface, confirming its sterility. In contrast, the positive control group disc displayed a surface covered by *S. aureus*, indicating the formation of biofilm on the surface. The disc that exhibited air-polishing treatment showed a little remaining *S. aureus* on the surface, suggesting fair decontamination. However, the discs treated with all other methods showed a clear surface, confirming the effective cleansability in successful decontamination.

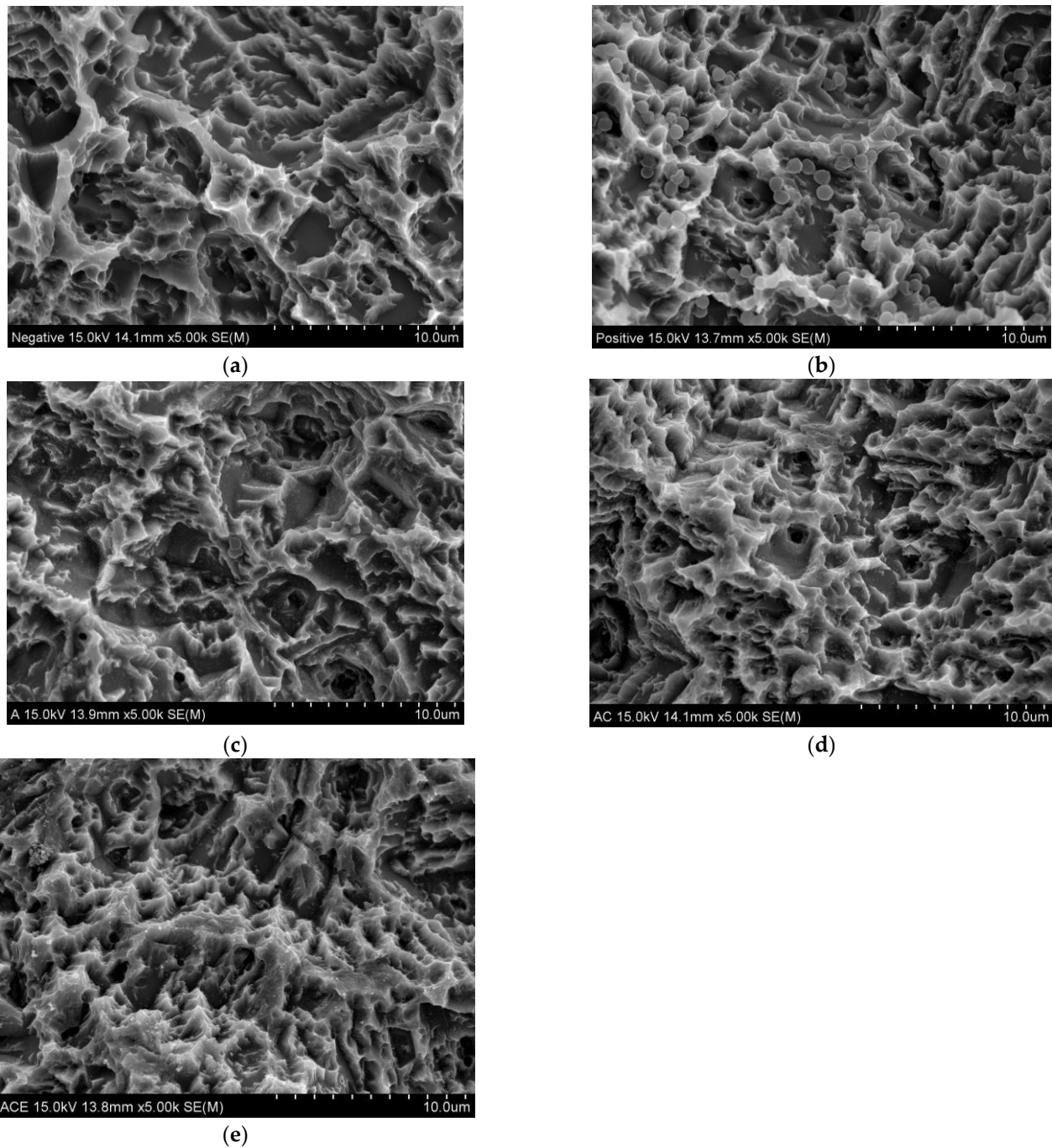


**Figure 5.** SEM images under a magnification of 5000× with 15.0 kV of groups (a) N, (b) P, (c) A, (d) AC, and (e) ACE.

### 3.2. Histologic Results

The tissue surrounding the disc in the experimental groups was magnified at 12.5× (Figure 6). The positive control group disc displayed a fibrous tissue gap between the disc and the cortical border. In contrast, the negative control group disc showed the osteoid and mineralized bone between the disc and the cortical border. The air-polishing treatment group disc exhibited the occupation of osteoid between the disc and the cortical border. The air-polishing treatment with chlorhexidine rinse group disc showed osteoid and mineralized bone between the disc and the cortical border. Finally, the air-polishing treatment with chlorhexidine rinse and Er:Yag laser treatment group disc showed the presence of mature mineralized bone between the disc and the cortical border.

### 3.3. FD Evaluation

The measured FDs of the ROI were analyzed using the Kruskal–Wallis test and showed statistically significant differences ( $p < 0.05$ ). For each group, the mean value and median value of FD were calculated (Table 2), and the differences among the groups indicated significant differences between groups P and N ( $p = 0.0246$ ), between groups P and AC ( $p = 0.0246$ ), and between groups P and ACE ( $p = 0.0196$ ) (Figure 7).

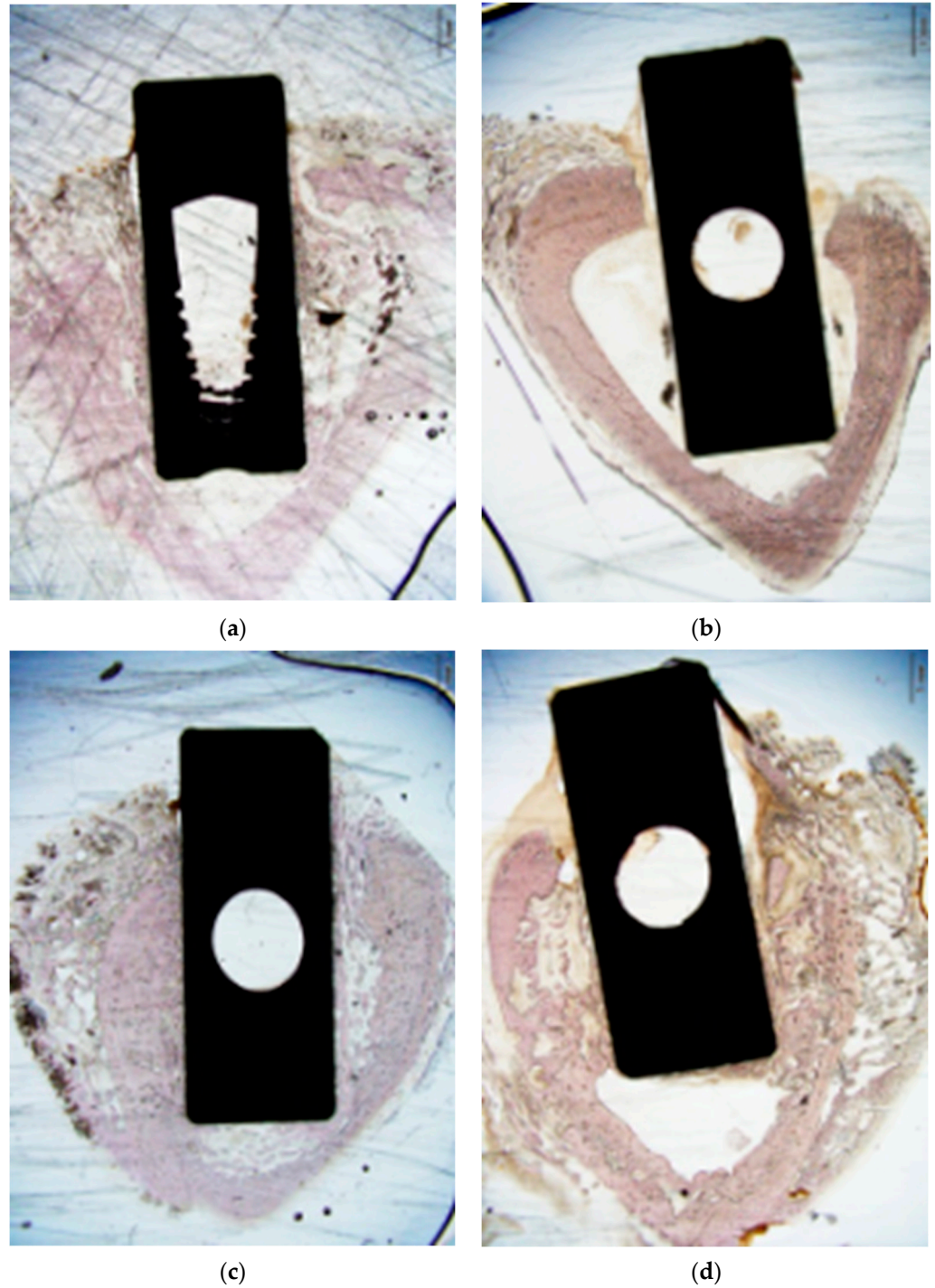


Figure 6. Cont.



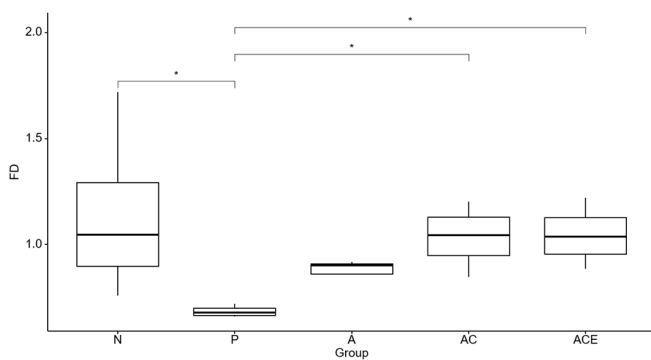


(e)

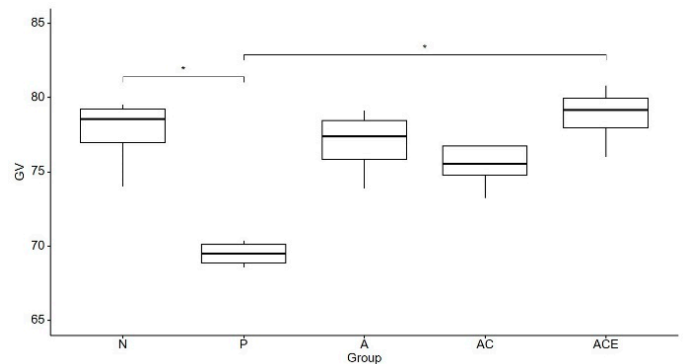
**Figure 6.** H&E-stained images under a magnification of 12.5× of groups (a) N, (b) P, (c) A, (d) AC, and (e) ACE.

**Table 2.** Measured FD of each group.

Group	Mean FD ( $\pm$ Standard Deviation)	Median FD (Interquartile Range)
N	1.1428 ( $\pm$ 0.4161)	1.0468 (0.3959)
P	0.6852 ( $\pm$ 0.0280)	0.6797 (0.0359)
A	0.8670 ( $\pm$ 0.0809)	0.9021 (0.0475)
AC	1.0337 ( $\pm$ 0.1544)	1.0436 (0.1819)
ACE	1.0455 ( $\pm$ 0.1454)	1.0375 (0.1726)



(a)



(b)

**Figure 7.** Comparison of (a) FDs across groups and (b) mean GVs across groups. \* indicates a statistically significant difference at  $p < 0.05$ .

### 3.4. Mean Grayscale Value Measurement

The mean GV of the ROI of the surrounding disc was measured for each group, and the mean value and median value are shown (Table 3). The Kruskal–Wallis test was used to compare the groups, and the results showed statistically significant differences ( $p < 0.05$ )

among the groups, namely, between groups P and N ( $p = 0.0382$ ) and between groups P and ACE ( $p = 0.0098$ ) (Figure 7).

**Table 3.** Measured GV of each group.

Group	Mean GV ( $\pm$ Standard Deviation)	Median GV (Interquartile Range)
N	77.6699 ( $\pm 2.5269$ )	78.5748 (2.2575)
P	69.4922 ( $\pm 0.8613$ )	69.5208 (1.2497)
A	76.9430 ( $\pm 2.3153$ )	77.3686 (2.6425)
AC	76.0333 ( $\pm 2.7649$ )	75.5185 (1.9444)
ACE	78.7824 ( $\pm 2.0657$ )	79.1574 (2.0424)

#### 4. Discussion

In the present study, we demonstrated the effectiveness of various decontamination treatments in removing biofilm from the surface of titanium discs and confirmed the formation of a bone matrix surrounding the discs. Furthermore, we measured the FD and mean GV obtained from the micro-CT scans after the implantation of these discs onto the tibia of rabbits. The purpose of the comparative analysis of the FD and mean GV was to assess the degree of osseointegration of the titanium discs, and we used the obtained values as reliable indicators of the extent of bone growth and density around the disc site.

Various treatments have been proposed in the literature for the effective decontamination of titanium implant surfaces. Decontamination using air-powder polishing, chlorhexidine, and lasers has shown significantly decreased bacterial colony-forming units [9,18,31]. Also, the air-abrasive system with glycine powder causes less alterations on a titanium surface [17,18].

In the current study, specimens that underwent different decontamination procedures were observed using SEM for the assessment of the surface tomography. The surface of the positive group was covered with *S. aureus*, indicating the biofilm formation. The effectiveness of different decontamination methods could be assessed by observing the remaining *S. aureus*. The results showed that the decontamination methods were effective for the removal of *S. aureus*.

For the evaluation of osseointegration, previous research on dogs revealed the success of treatment using an Er:YAG laser followed by saline irrigation and the air-polishing method. Also, the authors showed that the combination therapy of laser and chemical decontaminants, like chlorhexidine or saline solution, obtained higher osseointegration [20,32]. The effect of osseointegration depends on the bone matrix ingrowth and trabecular microstructures [33]. In this study, the results showed fair bone formation around the disc, as confirmed by the histologic images. We could observe osteoid and mineralized bone formation between the cortex and the disc. The micro-CT data were obtained to evaluate and quantify the degree of osseointegration.

The data acquired from the micro-CT scans and histological specimens were compared to evaluate the accordance between them, and the difference between the two techniques was not statistically significant. Based on this, the results from the micro-CT scans were consistent with the results from the histophotomicrograph images [30]. The images corresponding to the histologic specimen images in the micro-CT data were collected for the selection of the ROI and fractal analysis, confirming the formation of trabecular bone in both data. The ROI was placed between the disc and the cortical border of the tibia that excluded the disc. Other studies have reported a greater emphasis on the location of the ROI for fractal analysis than on its size [34]. A rectangle of  $25 \times 100$  pixels was selected as the ROI, considering the thickness between the cortex and the disc.

FD has been used for the assessment of osteoporosis, bone healing, periodontitis, and the stability of implants on radiographs [25,34–36]. It is a well-known method for investigating bone mineral density (BMD), where higher box-counting values imply complex trabecular and medullar bone. Also, a decrease in bone density corresponds to a decrease in FD [37,38]. It was previously reported that the trabecular patterns became thickened and

radiographic features changed in the bone implant interface [25]. In a study comparing the FD of pre- and post-implants, an increased fractal dimension of the post-implant was reported, and a decrease in the FD was observed in a failed implant [34].

In this study, the mean value of the FD in all experimental groups and the negative control group showed a higher value than that of the positive control group. The decreased FD of the positive control group suggested decreased bone density and a trabecular pattern surrounding the disc. The mean value of the FD in the negative control group and the decontaminated discs with air-polishing treatment, chlorhexidine rinse, and additional Er:Yag laser treatment showed a statistically significant difference compared to the positive control group, but the difference among the groups was insignificant. This result implies an increase in the bone structure and trabeculae around the discs in the groups AC, ACE, and N compared to the contaminated discs.

Bone density evaluation using computed tomography (CT) is based on radiological density and depends on the attenuation of X-ray beams by the type of tissue [39]. The BMD of a region of interest can be quantified as an average of the grayscale value, and a low grayscale value indicates a low bone density [40]. The density estimations using both two-dimensional and three-dimensional methods showed statistically insignificant differences [41].

In the current study, the mean GV was measured based on three-dimensionally reconstructed segmentation. The segmentation consisted of an additional 20 pixels surrounding the disc to include the trabecular pattern. The mean GV values of all experimental groups and the negative control group were higher than those of the positive control group, implying decreased bone density of the segmentation surrounding the discs. The mean values of the GV of the negative control group and the decontaminated discs with air-polishing treatment, chlorhexidine rinse, and Er:Yag laser treatment showed statistically significant differences compared to the positive control group, but there was an insignificant difference between the two groups. The result indicates an increase in bone density in the negative control group and the decontaminated discs with air polishing treatment, chlorhexidine rinse, and Er:Yag laser treatment compared to the contaminated discs.

There are some limitations in the present study. Threshold settings for bone and objects, such as implants and discs, are major procedures in micro-CT analysis. In this study, thresholds were set for titanium and bone, within the possibilities of variance due to experimental conditions and characteristic differences among individual specimens [42]. In addition, the ROI for evaluation was determined according to the titanium disc threshold, and there was a possibility that the value of ROI might differ due to the threshold set for bone. Due to the small sample size, there is still a limitation in terms of the statistical verification of individual specimen differences. Also, the analysis of the images corresponding to the histologic images obtained from micro-CT was performed manually, which could lead to inaccuracy. There are different methods used for the calculation of FD, and the box-counting method, which was employed in this research, is one of the most commonly used, although there is no consensus on the gold standards [43].

Despite the limitations, only a few studies have reported the osseointegration of decontaminated titanium discs including dental implants, and there are various methods used for decontamination, leading to a lack of evidence for a universal decontamination method. The present study examined decontaminated titanium discs to investigate the surface decontamination and osseointegration of these discs. The SEM images could confirm the status of covered *S. aureus* in the experimental groups, and the histologic specimens showed favorable bone formation. Furthermore, the quantitative investigation using FD and GV based on micro-CT images for assessing bone structures and quality showed statistically significant differences among the experimental groups. Specifically, the negative control group and the decontaminated discs after air-polishing treatment with chlorhexidine rinse and Er:Yag laser treatment showed statistically significantly higher values than the contaminated discs in both investigations. For further studies, clinical evaluations

of osseointegration in concordance with radiographic features could be investigated to address the degree of osseointegration of contaminated titanium implants.

## 5. Conclusions

The decontamination method using air polishing treatment with chlorhexidine rinse and an Er:Yag laser showed effectiveness in the removal of biofilm and osseointegration in rabbits. The FD analysis and mean GV analysis results showed higher values than those of contaminated discs. These radiographic analyses could be used in assessing bone trabecular patterns around discs in different situations. Although these results may be regarded as preliminary, higher FD and GV values may indicate an increase in bone density and successful osseointegration.

**Author Contributions:** Conceptualization, H.-J.P.; methodology, H.-J.P. and J.-K.K.; validation, H.J.K., J.-K.K. and H.-J.P.; formal analysis, H.J.K. and Y.K.L.; investigation, H.J.K., K.C. and J.H.K.; data curation, H.J.K., K.C. and C.P.; writing—original draft preparation, H.J.K.; writing—review and editing, H.J.K., J.R., S.J., M.-S.K. and H.-J.P.; visualization, H.J.K.; supervision, H.-J.P. and H.-K.O.; project administration, H.-J.P. All authors have read and agreed to the published version of the manuscript.

**Funding:** This study was supported by a grant (BCRI21031, B2021-0049) from the Chonnam National University Hospital Biomedical Research Institute.

**Institutional Review Board Statement:** The present study was reviewed and approved by the Institutional Animal Care and Use Committee of Chonnam National University Hospital (approval number: CNUHIACUC-22017).

**Informed Consent Statement:** Not applicable.

**Data Availability Statement:** The datasets used and/or analyzed during the current study are available from the corresponding author upon reasonable request.

**Conflicts of Interest:** The authors declare no conflict of interest.

## References

- Madi, M.; Htet, M.; Zakaria, O.; Alagl, A.; Kasugai, S. Re-osseointegration of Dental Implants After Periimplantitis Treatments: A Systematic Review. *Implant Dent.* **2018**, *27*, 101–110. [[CrossRef](#)] [[PubMed](#)]
- Parlar, A.; Bosshardt, D.D.; Cetiner, D.; Schafroth, D.; Unsal, B.; Haytaç, C.; Lang, N.P. Effects of decontamination and implant surface characteristics on re-osseointegration following treatment of peri-implantitis. *Clin. Oral Implant. Res.* **2009**, *20*, 391–399. [[CrossRef](#)] [[PubMed](#)]
- Batalha, V.C.; Bueno, R.A.; Fronchetti Junior, E.; Mariano, J.R.; Santin, G.C.; Freitas, K.M.S.; Ortiz, M.A.L.; Salmeron, S. Dental Implants Surface in vitro Decontamination Protocols. *Eur. J. Dent.* **2021**, *15*, 407–411. [[CrossRef](#)] [[PubMed](#)]
- Berglundh, T.; Jepsen, S.; Stadlinger, B.; Terheyden, H. Peri-implantitis and its prevention. *Clin. Oral Implant. Res.* **2019**, *30*, 150–155. [[CrossRef](#)]
- Schwarz, F.; Sahm, N.; Iglhaut, G.; Becker, J. Impact of the method of surface debridement and decontamination on the clinical outcome following combined surgical therapy of peri-implantitis: A randomized controlled clinical study. *J. Clin. Periodontol.* **2011**, *38*, 276–284. [[CrossRef](#)]
- Lindhe, J.; Meyle, J. Peri-implant diseases: Consensus Report of the Sixth European Workshop on Periodontology. *J. Clin. Periodontol.* **2008**, *35*, 282–285. [[CrossRef](#)]
- Mellado-Valero, A.; Buitrago-Vera, P.; Solá-Ruiz, M.F.; Ferrer-García, J.C. Decontamination of dental implant surface in peri-implantitis treatment: A literature review. *Med. Oral Patol. Oral Cir. Bucal* **2013**, *18*, e869–e876. [[CrossRef](#)]
- Salmeron, S.; Rezende, M.L.; Consolaro, A.; Sant’ana, A.C.; Damante, C.A.; Greggi, S.L.; Passanezi, E. Laser therapy as an effective method for implant surface decontamination: A histomorphometric study in rats. *J. Periodontol.* **2013**, *84*, 641–649. [[CrossRef](#)]
- Marotti, J.; Tortamano, P.; Cai, S.; Ribeiro, M.S.; Franco, J.E.; de Campos, T.T. Decontamination of dental implant surfaces by means of photodynamic therapy. *Lasers Med. Sci.* **2013**, *28*, 303–309. [[CrossRef](#)]
- Moharrami, M.; Perrotti, V.; Iaculli, F.; Love, R.M.; Quaranta, A. Effects of air abrasive decontamination on titanium surfaces: A systematic review of in vitro studies. *Clin. Implant Dent. Relat. Res.* **2019**, *21*, 398–421. [[CrossRef](#)]
- Fraga, R.S.; Antunes, L.A.A.; Fontes, K.; Küchler, E.C.; Iorio, N.; Antunes, L.S. Is Antimicrobial Photodynamic Therapy Effective for Microbial Load Reduction in Peri-implantitis Treatment? A Systematic Review and Meta-Analysis. *Photochem. Photobiol.* **2018**, *94*, 752–759. [[CrossRef](#)] [[PubMed](#)]

12. Schou, S.; Holmstrup, P.; Skovgaard, L.T.; Stoltze, K.; Hjorting-Hansen, E.; Wenzel, A.; Jørgensen, T. Implant surface preparation in the surgical treatment of experimental peri-implantitis with autogenous bone graft and ePTFE membrane in cynomolgus monkeys. *Clin. Oral Implant. Res.* **2003**, *14*, 412–422. [[CrossRef](#)] [[PubMed](#)]
13. Schou, S.; Berglundh, T.; Lang, N.P. Surgical treatment of peri-implantitis. *Int. J. Oral Maxillofac. Implant.* **2004**, *19*, 140–149.
14. Meyle, J. Mechanical, chemical and laser treatments of the implant surface in the presence of marginal bone loss around implants. *Eur. J. Oral Implantol.* **2012**, *5*, S71–S81. [[PubMed](#)]
15. Fenelon, T.; Bakr, M.M.; Walsh, L.J.; George, R. Effects of Lasers and Their Delivery Characteristics on Machined and Micro-Roughened Titanium Dental Implant Surfaces. *Bioengineering* **2020**, *7*, 93. [[CrossRef](#)]
16. Valderrama, P.; Wilson, T.G., Jr. Detoxification of implant surfaces affected by peri-implant disease: An overview of surgical methods. *Int. J. Dent.* **2013**, *2013*, 740680. [[CrossRef](#)]
17. Baima, G.; Citterio, F.; Romandini, M.; Romano, F.; Mariani, G.M.; Buduneli, N.; Aimetti, M. Surface decontamination protocols for surgical treatment of peri-implantitis: A systematic review with meta-analysis. *Clin. Oral Implant. Res.* **2022**, *33*, 1069–1086. [[CrossRef](#)] [[PubMed](#)]
18. Cochis, A.; Fini, M.; Carrassi, A.; Migliario, M.; Visai, L.; Rimondini, L. Effect of air polishing with glycine powder on titanium abutment surfaces. *Clin. Oral Implant. Res.* **2013**, *24*, 904–909. [[CrossRef](#)]
19. Pranno, N.; Cristalli, M.P.; Mengoni, F.; Sauzullo, I.; Annibali, S.; Polimeni, A.; La Monaca, G. Comparison of the effects of air-powder abrasion, chemical decontamination, or their combination in open-flap surface decontamination of implants failed for peri-implantitis: An ex vivo study. *Clin. Oral Investig.* **2021**, *25*, 2667–2676. [[CrossRef](#)]
20. Subramani, K.; Wismeijer, D. Decontamination of titanium implant surface and re-osseointegration to treat peri-implantitis: A literature review. *Int. J. Oral Maxillofac. Implant.* **2012**, *27*, 1043–1054.
21. Ishikawa, I.; Aoki, A.; Takasaki, A.A. Potential applications of Erbium:YAG laser in periodontics. *J. Periodontal Res.* **2004**, *39*, 275–285. [[CrossRef](#)] [[PubMed](#)]
22. Kreisler, M.; Kohnen, W.; Marinello, C.; Götz, H.; Duschner, H.; Jansen, B.; D’Hoedt, B. Bactericidal Effect of the Er:YAG Laser on Dental Implant Surfaces: An In Vitro Study. *J. Periodontol.* **2002**, *73*, 1292–1298. [[CrossRef](#)] [[PubMed](#)]
23. Gosau, M.; Hahnel, S.; Schwarz, F.; Gerlach, T.; Reichert, T.E.; Bürgers, R. Effect of six different peri-implantitis disinfection methods on in vivo human oral biofilm. *Clin. Oral Implant. Res.* **2010**, *21*, 866–872. [[CrossRef](#)]
24. Wetzel, A.C.; Vlassis, J.; Caffesse, R.G.; Hämmerle, C.H.; Lang, N.P. Attempts to obtain re-osseointegration following experimental peri-implantitis in dogs. *Clin. Oral Implant. Res.* **1999**, *10*, 111–119. [[CrossRef](#)]
25. Lubis, R.T.; Azhari, A.; Pramanik, F. Analysis of Bone Density and Bone Morphometry by Periapical Radiographs in Dental Implant Osseointegration Process. *Int. J. Dent.* **2023**, *2023*, 4763961. [[CrossRef](#)]
26. Sener, E.; Cinarcik, S.; Baksi, B.G. Use of Fractal Analysis for the Discrimination of Trabecular Changes Between Individuals with Healthy Gingiva or Moderate Periodontitis. *J. Periodontol.* **2015**, *86*, 1364–1369. [[CrossRef](#)] [[PubMed](#)]
27. Abdulhameed, E.A.; Al-Rawi, N.H.; Uthman, A.T.; Samsudin, A.R. Bone Texture Fractal Dimension Analysis of Ultrasound-Treated Bone around Implant Site: A Double-Blind Clinical Trial. *Int. J. Dent.* **2018**, *2018*, 2672659. [[CrossRef](#)]
28. Shrout, M.K.; Potter, B.J.; Hildebolt, C.F. The effect of image variations on fractal dimension calculations. *Oral Surg. Oral Med. Oral Pathol. Oral Radiol. Endodontol.* **1997**, *84*, 96–100. [[CrossRef](#)]
29. Khojastepour, L.; Mohammadzadeh, S.; Jazayeri, M.; Omidi, M. In vitro Evaluation of the Relationship between Gray Scales in Digital Intraoral Radiographs and Hounsfield Units in CT Scans. *J. Biomed. Phys. Eng.* **2017**, *7*, 289–298.
30. Das, S.; Dholam, K.; Gurav, S.; Bendale, K.; Ingle, A.; Mohanty, B.; Chaudhari, P.; Bellare, J.R. X-ray computed microtomography datasets for osteogenic nanofibrous coated titanium implants. *Sci. Data* **2022**, *9*, 348. [[CrossRef](#)]
31. Otsuki, M.; Wada, M.; Yamaguchi, M.; Kawabata, S.; Maeda, Y.; Ikebe, K. Evaluation of decontamination methods of oral biofilms formed on screw-shaped, rough and machined surface implants: An ex vivo study. *Int. J. Implant Dent.* **2020**, *6*, 18. [[CrossRef](#)] [[PubMed](#)]
32. Solderer, A.; Pippenger, B.E.; Donnet, M.; Wiedemeier, D.; Ramenzoni, L.L.; Schmidlin, P.R. Evaluation of air polishing with a sterile powder and mechanical debridement during regenerative surgical periimplantitis treatment: A study in dogs. *Clin. Oral Investig.* **2021**, *25*, 2609–2618. [[CrossRef](#)] [[PubMed](#)]
33. Lyu, L.; Yang, S.; Jing, Y.; Zhang, C.; Wang, J. Examining trabecular morphology and chemical composition of peri-scaffold osseointegrated bone. *J. Orthop. Surg. Res.* **2020**, *15*, 406. [[CrossRef](#)] [[PubMed](#)]
34. Sansare, K.; Singh, D.; Karjodkar, F. Changes in the fractal dimension on pre- and post-implant panoramic radiographs. *Oral Radiol.* **2012**, *28*, 15–23. [[CrossRef](#)]
35. Heo, M.S.; Park, K.S.; Lee, S.S.; Choi, S.C.; Koak, J.Y.; Heo, S.J.; Han, C.H.; Kim, J.D. Fractal analysis of mandibular bony healing after orthognathic surgery. *Oral Surg. Oral Med. Oral Pathol. Oral Radiol. Endodontol.* **2002**, *94*, 763–767. [[CrossRef](#)]
36. Law, A.N.; Bollen, A.M.; Chen, S.K. Detecting osteoporosis using dental radiographs: A comparison of four methods. *J. Am. Dent. Assoc.* **1996**, *127*, 1734–1742. [[CrossRef](#)]
37. Hayek, E.; Aoun, G.; Geha, H.; Nasseh, I. Image-based Bone Density Classification Using Fractal Dimensions and Histological Analysis of Implant Recipient Site. *Acta Inform. Med.* **2020**, *28*, 272–277. [[CrossRef](#)]
38. Southard, T.E.; Southard, K.A.; Jakobsen, J.R.; Hillis, S.L.; Najim, C.A. Fractal dimension in radiographic analysis of alveolar process bone. *Oral Surg. Oral Med. Oral Pathol. Oral Radiol. Endodontol.* **1996**, *82*, 569–576. [[CrossRef](#)]

39. Morar, L.; Băciuț, G.; Băciuț, M.; Bran, S.; Colosi, H.; Manea, A.; Almășan, O.; Dinu, C. Analysis of CBCT Bone Density Using the Hounsfield Scale. *Prosthesis* **2022**, *4*, 414–423. [[CrossRef](#)]
40. Tu, S.J.; Wang, S.P.; Cheng, F.C.; Chen, Y.J. Extraction of gray-scale intensity distributions from micro computed tomography imaging for femoral cortical bone differentiation between low-magnesium and normal diets in a laboratory mouse model. *Sci. Rep.* **2019**, *9*, 8135. [[CrossRef](#)]
41. Genisa, M.; Shuib, S.; Rajion, Z.A.; Arief, E.M.; Hermana, M. Density estimation based on the Hounsfield unit value of cone beam computed tomography imaging of the jawbone system. *Proc. Inst. Mech. Eng. H* **2018**, *232*, 1168–1175. [[CrossRef](#)] [[PubMed](#)]
42. Hong, J.-M.; Kim, U.-G.; Yeo, I.-S.L. Comparison of three-dimensional digital analyses and two-dimensional histomorphometric analyses of the bone-implant interface. *PLoS ONE* **2022**, *17*, e0276269. [[CrossRef](#)] [[PubMed](#)]
43. Mishra, S.; Kumar, M.; Mishra, L.; Mohanty, R.; Nayak, R.; Das, A.C.; Mishra, S.; Panda, S.; Lapinska, B. Fractal Dimension as a Tool for Assessment of Dental Implant Stability-A Scoping Review. *J. Clin. Med.* **2022**, *11*, 4051. [[CrossRef](#)] [[PubMed](#)]

**Disclaimer/Publisher's Note:** The statements, opinions and data contained in all publications are solely those of the individual author(s) and contributor(s) and not of MDPI and/or the editor(s). MDPI and/or the editor(s) disclaim responsibility for any injury to people or property resulting from any ideas, methods, instructions or products referred to in the content.